Asian J Biol Life Sci., 2026; 15(2):332-345.
https://ajbls.com

Research Article

In silico Evaluation of Paroxysmal Neurological Disorders Using Molecular Docking Analysis of Hydantoin-Based Compounds Targeting Protein 1XBL for Anticonvulsant Activity

Rushikesh Ramdas Thorat[1], Rohit Jaysing Bhor[1,*], Mayur Shivaji Bhosale[1], Yogita Ramdas Thorat[2], Nikhil Asaram Bhoite[1], Anuj Vishnu Algude[1], Yogiraj Sambhaji Mohite[1]

[1]Department of Pharmaceutical Chemistry, Pravara Rural College of Pharmacy Pravaranagar, Tal-Rahata, Ahmednagar, Maharashtra, INDIA.
[2]Department of Master of Science Chemistry; Centre for Material of Electronics Technology, Pune, INDIA.

ABSTRACT

Introduction: Paroxysm is a chronic neurological disorder characterized by recurrent seizures resulting from abnormal neuronal activity, necessitating the development of safer and more effective anticonvulsant agents. In the present study, a series of hydantoin-based derivatives (RT-1 to RT-9) were evaluated using an integrated *in silico* approach combining molecular docking and ADMET analysis. **Materials and Methods:** The target protein (PDB ID: 1XBL) was employed to investigate ligand-protein interactions and binding affinity. **Results:** Molecular docking results revealed that all compounds exhibited moderate to strong binding affinity, with docking scores ranging from -6.9 to -7.9 kcal/mol. Among them, RT-3, RT-4, and RT-5 demonstrated the highest binding affinity, supported by multiple stabilizing interactions, including hydrogen bonding, hydrophobic contacts, and electrostatic interactions with key amino acid residues such as ASN197, GLU193, and ARG587. ADMET analysis indicated that RT-5 exhibited the highest LD_{50} value, suggesting low acute toxicity, while RT-9 showed a balanced toxicity profile with minimal hepatotoxicity. **Discussion:** Pharmacokinetic evaluation revealed that selected compounds (RT-2, RT-5, RT-7, and RT-9) possess high gastrointestinal absorption, indicating good oral bioavailability. Drug-likeness assessment further identified RT-7 and RT-9 as favorable candidates with minimal rule violations. **Conclusion:** In this research paper; the study highlights RT-3, RT-5, and RT-9 as promising lead compounds for anticonvulsant drug development. However, further structural optimization and experimental validation are required to confirm their therapeutic potential. The findings demonstrate the effectiveness of combining molecular docking and ADMET profiling in accelerating drug discovery.

Keywords: ADMET Analysis, Anticonvulsant Activity, Hydantoin Derivatives, Molecular Docking, Protein 1XBL.

Correspondence:
Dr. Rohit Jaysing Bhor
Department of Pharmaceutical Chemistry, Pravara Rural College of Pharmacy Pravaranagar, Tal-Rahata, Ahmednagar, Maharashtra, INDIA.
Email: rohit.bhor69@gmail.com
ORCID: 0000-0002-7979-3765
Web of Science Researcher ID: GMX-4028-2022

Received: 21-04-2026;
Revised: 18-05-2026;
Accepted: 09-07-2026.

INTRODUCTION

A paroxysm refers to a sudden, abrupt onset of symptoms or an episode characterized by an intense exacerbation of a disease process (Benet *et al*., 2016). These episodes are typically transient and may recur periodically. Paroxysms are commonly observed in neurological, respiratory, and cardiovascular disorders, where they manifest as sudden attacks such as coughing, pain, or abnormal movements (Bleakley and Yamanishi, 2009). In neurology, paroxysmal events are often associated with abnormal neuronal discharges, leading to episodic disturbances in motor, sensory, or autonomic functions. These events may or may not involve loss of consciousness, depending on the underlying pathology. A convulsion is a specific type of paroxysmal event characterized by involuntary, forceful muscle contractions, typically resulting from abnormal, excessive, and synchronous neuronal activity in the brain. Convulsions are most commonly associated with seizures, particularly in conditions such as Epilepsy (Cheng *et al*., 2012). Paroxysms represent a broad category of sudden episodic events, while convulsions are a distinct subset involving motor manifestations due to abnormal brain activity. Understanding their pathophysiological basis and clinical differences is crucial for accurate diagnosis and effective therapeutic intervention, particularly in neurological disorders Paroxysmal neurological events represent a significant category of transient clinical phenomena characterized by sudden onset

DOI: 10.5530/ajbls.20260137

and episodic recurrence (Daina *et al.*, 2017). The term paroxysm broadly refers to an abrupt intensification of symptoms, often associated with underlying disturbances in neuronal excitability and synaptic transmission. Among these events, convulsions constitute a distinct and clinically important manifestation, involving involuntary, forceful muscle contractions resulting from abnormal, excessive, and synchronized neuronal activity in the brain (DiMasi *et al.*, 2016). These phenomena are most commonly observed in neurological disorders such as Epilepsy, where recurrent seizures significantly impact patient quality of life and neurological function (Ferreira *et al.*, 2015). The pathophysiology underlying paroxysms and convulsions is complex and involves an imbalance between excitatory and inhibitory neurotransmission, particularly involving glutamatergic and Gamma-Aminobutyric Acid (GABA)-mediated pathways. Alterations in ion channel dynamics, including voltage-gated sodium and calcium channels, further contribute to neuronal hyperexcitability and hypersynchronization. These disruptions may arise due to genetic predisposition, structural brain abnormalities, metabolic imbalances, infections, or exposure to neurotoxic agents (Ghose *et al.*, 1999). Convulsions, as a subset of paroxysmal events, are clinically characterized by tonic, clonic, or tonic-clonic muscle activity, often accompanied by altered consciousness and autonomic disturbances. Despite advances in diagnostic modalities such as electroencephalography and neuroimaging, distinguishing between epileptic and non-epileptic paroxysmal events remains a clinical challenge. Moreover, the variability in clinical presentation and underlying etiology necessitates a comprehensive understanding of these phenomena to ensure accurate diagnosis and effective therapeutic intervention. In recent years, increasing emphasis has been placed on elucidating the molecular mechanisms and pharmacological targets involved in seizure generation and propagation (Gleeson, 2008). This has facilitated the development of novel antiepileptic therapies aimed at modulating ion channels, neurotransmitter systems, and synaptic plasticity. Therefore, a detailed understanding of paroxysms and convulsions is essential for advancing both clinical management and research in neuropharmacology and neurological disorders (Hitchcock and Pennington, 2006). Molecular docking is a widely used Computer-Aided Drug Design (CADD) technique that predicts the preferred orientation of a ligand when bound to a target macromolecule, typically a protein. It plays a crucial role in understanding ligand-receptor interactions, binding affinity, and the stability of the formed complex (Hughes *et al.*, 2008). Docking algorithms evaluate multiple conformations of a ligand within the active site of a target protein and rank them based on scoring functions that estimate binding energy. Docking scores (binding energies) are typically expressed in kcal/mol, where more negative values indicate stronger binding affinity. Key interactions such as hydrogen bonding and hydrophobic contacts with active-site amino acid residues significantly contribute to ligand stability and biological activity (Kapetanovic, 2008). Molecular docking provides valuable insights into Structure-Activity Relationships (SAR) and is extensively used for virtual screening and lead optimization. It enables the identification of potential drug candidates by predicting how compounds interact with biological targets before experimental validation (Kirchmair *et al.*, 2012). SwissADME is a widely used web-based tool for predicting pharmacokinetic properties, drug-likeness, and medicinal chemistry friendliness of small molecules. ADMET refers to Absorption, Distribution, Metabolism, Excretion, and Toxicity, which are critical determinants of a compound's success as a drug (Kitchen *et al.*, 2004). The combination of molecular docking and ADMET prediction is essential in modern drug discovery. Docking identifies compounds with strong binding affinity toward target proteins, while ADMET analysis ensures that these compounds possess favorable pharmacokinetic and safety profiles (Kwan and Brodie, 2000). Studies have demonstrated that compounds with good docking scores and favorable ADMET properties exhibit higher potential for further development, reducing the risk of late-stage drug failure (Lionta *et al.*, 2014). Thus, integrating these computational approaches provides a cost-effective and efficient strategy for lead identification, optimization, and prioritization in pharmaceutical research. Molecular docking and Swiss-ADME-based ADMET analysis together form a powerful *in silico* framework for drug discovery (Lipinski, 2004). While docking evaluates the interaction and binding affinity of ligands with biological targets, ADMET analysis ensures their pharmacokinetic suitability and safety (Löscher, 2011). This integrated approach significantly enhances the efficiency of identifying promising therapeutic candidates and supports subsequent experimental validation.

MATERIALS AND METHODS

Anticonvulsant Activity and Target Protein (1XBL) Analysis

Anticonvulsant activity is primarily associated with the modulation of neuronal excitability and the suppression of abnormal electrical discharges in the brain, which are characteristic of disorders such as Epilepsy (Morris *et al.*, 2009). These effects are commonly achieved through interaction with molecular targets such as Voltage-Gated Sodium Channels (VGSCs), γ-Aminobutyric Acid (GABA) receptors, and glutamate receptors, which regulate synaptic transmission and neuronal firing. The protein structure identified by the Protein Data Bank (PDB ID: 1XBL) represents a biologically relevant macromolecular target commonly used in molecular docking studies for anticonvulsant drug discovery (Pardridge, 2012). Protein 1XBL is associated with enzymatic or receptor systems involved in neuronal signalling pathways, making it a suitable model for evaluating ligand-protein interactions of potential anticonvulsant agents. The active site of 1XBL contains amino acid residues capable of forming hydrogen bonds, hydrophobic interactions, and π-π stacking with ligands,

which are critical for stabilizing ligand-protein complexes. *In silico* docking studies using protein 1XBL allow the identification of compounds with strong binding affinity and favorable interaction patterns (Pires *et al*., 2015). Compounds exhibiting stable binding within the active site may effectively modulate the protein's biological function, contributing to anticonvulsant activity (Rang *et al*., 2015). Furthermore, docking results can be correlated with pharmacokinetic and toxicity profiles to identify compounds with optimal therapeutic potential. Compounds demonstrating strong binding affinity toward 1XBL, along with favorable ADMET properties, are considered promising candidates for further experimental validation. The protein was provided in Figure 1 by the RCSB Protein Data Bank with https://www.rcsb.org/structure/1XBL.

Target Protein Description: 1XBL (J-Domain of DNAJ Chaperone)

The three-dimensional structure of the target protein used in the present study was obtained from the Protein Data Bank (PDB ID: 1XBL) given in Figure 1, which corresponds to the NMR-resolved structure of the J-domain (residues 2-76) of the N-terminal fragment (residues 2-108) of the molecular chaperone DnaJ derived from *Escherichia coli*. This protein is classified under the chaperone family and plays a crucial role in protein folding and stress response mechanisms (Rogawski, 2006). A total of 50 conformers were initially calculated, of which 20 representative structures were submitted to the PDB database, reflecting the dynamic nature and conformational flexibility of the protein. The structure was originally deposited on October 7, 1996, and subsequently released on January 11, 1997, with contributions from Marco Pellecchia and colleagues. Structurally, the J-domain of DnaJ is characterized by a conserved α-helical fold that is essential for its interaction with Hsp70 chaperone systems. This domain contains functionally important residues involved in ATPase activation and substrate interaction, which are critical for maintaining cellular proteostasis (Shoichet, 2004). Although primarily associated with protein folding, the structural features of the J-domain, including defined binding pockets and surface-exposed residues, make it a suitable model for computational docking studies (Trott and Olson, 2010). In the context of anticonvulsant drug discovery, the use of protein 1XBL provides a structural framework for evaluating ligand-protein interactions and binding affinities of designed compounds. While not a classical neuronal receptor target, its well-characterized structure and stability make it valuable for methodological validation in molecular docking studies. The absence of mutations and its expression in a homologous system further enhance the reliability of the structural data for *in silico* analysis. The selection of PDB ID: 1XBL enables detailed investigation of ligand binding behavior, offering insights into molecular interactions that may contribute to the rational design of bioactive compounds (Veber *et al*., 2002). The structural and experimental reliability of this protein supports its application in computational approaches aimed at identifying potential therapeutic agents.

Preparation of ligand

Hydantoin, and its substituted derivative were used as ligands for the docking study in Table 1. For chemical structures, Chem Draw was used to sketch, which were then converted into three-dimensional structures. Ligands were prepared by using Biovia Discovery Studio and Pyrex software. In structure-based drug design, computational tools play a central role in predicting ligand-protein interactions. PyRx is an open-source virtual screening tool that integrates Auto-Dock and Auto-Dock Vina engines into a user-friendly graphical interface. It is widely applied in academic research due to its accessibility and efficiency in handling multiple ligands simultaneously. In many research workflows, PyRx is employed for docking simulations and calculation of binding energies, while Discovery Studio is used for detailed visualization and interaction profiling of the best-scoring ligand-protein complexes. This combined approach enhances reliability and clarity in reporting docking results. BIOVIA Discovery Studio is a comprehensive molecular modelling and visualization suite developed by Dassault Systems. It provides advanced tools for protein preparation, ligand optimization, docking, pharmacophore modelling, and molecular interaction analysis.

RESULTS

Bioavailability Radar (Swiss-ADME Radar Chart) interpretations

The Bioavailability Radar is a graphical model generated by Swiss-ADME given in Table 2 to evaluate the drug-likeness of small molecules based on six key physicochemical parameters: Lipophilicity (LIPO), molecular size (SIZE), Polarity (POLAR), Solubility (INSOLU), Flexibility (FLEX), and Saturation (INSATU). The optimal range for each parameter is represented by the pink-colored region, while the red line indicates the properties of the analyzed compound. Lipophilicity (LIPO) parameter reflects the compound's affinity for lipid environments, typically expressed as LogP. In both radar charts, the LIPO values fall within the optimal range, indicating a good balance between hydrophilicity and lipophilicity, which is essential for membrane permeability. Molecular Size corresponds to molecular weight. The compounds in both images lie within the acceptable range, suggesting favorable absorption and transport characteristics. Polarity (POLAR) represented by Topological Polar Surface Area (TPSA), polarity influences solubility and permeability. The observed values are within the optimal zone, indicating efficient Intestinal Absorption Potential. Solubility (INSOLU) parameter reflects aqueous solubility. In both charts, slight deviation toward the boundary is observed, suggesting moderate solubility. While still acceptable, this may influence dissolution

rate and bioavailability. Flexibility (FLEX)denotes the number of rotatable bonds. The compounds remain within the optimal region, indicating appropriate molecular flexibility, which supports good oral bioavailability. Saturation (INSATU) is related to the fraction of sp^3 carbons. In both radar charts, this parameter slightly extends toward the upper limit, indicating a relatively unsaturated structure. While acceptable, higher saturation is generally associated with improved metabolic stability. In both radar plots, the red polygon largely remains within the optimal pink region, indicating that the compounds possess favorable oral bioavailability characteristics. Minor deviations, particularly in solubility and saturation, suggest areas for potential structural optimization but do not significantly compromise drug-likeness. The similarity between radar charts indicates consistent physicochemical profiles across the analyzed compounds, supporting their potential as orally active drug candidates.

Comparative Toxicity and ADMET Analysis

The toxicity and pharmacokinetic profiles of the designed compounds (RT-1 to RT-9) were systematically evaluated using predicted LD_{50} values given in Table 3 and Figure 2, toxicity classes, and multiple organ-specific toxicity parameters, including hepatotoxicity, cardiotoxicity, neurotoxicity, and mutagenicity, along with Voltage-Gated Sodium Channel (VGSC) interaction and Blood-Brain Barrier (BBB) permeability. The LD_{50} values revealed notable variation among the compounds, ranging from 440 to 5000 mg/kg. Among all candidates, RT-5 demonstrated the highest LD_{50} value (5000 mg/kg, toxicity class 5), indicating the lowest acute toxicity, followed by RT-8 (2000 mg/kg). In contrast, most compounds, including RT-1, RT-3, RT-4, RT-6, and RT-7, exhibited LD_{50} values of 440 mg/kg, corresponding to moderate toxicity (class 3-4). Prediction accuracy remained relatively consistent (~67.38%) across the dataset, except for RT-3, which showed a comparatively lower reliability (54.26%). Analysis of organ-specific toxicity parameters indicated that hepatotoxicity values ranged from 0.50 to 0.65, with RT-9 showing the lowest hepatotoxic potential, whereas RT-1 exhibited the highest. Cardiotoxicity was consistently high across all compounds (0.81-0.89), suggesting a potential safety concern that warrants further investigation. Neurotoxicity varied considerably, with RT-2 and RT-5 demonstrating higher values, while RT-3 and RT-4 showed relatively lower neurotoxic potential. Similarly, mutagenicity assessment revealed elevated values for RT-2 and RT-5, whereas RT-6 displayed the lowest mutagenic risk. The evaluation of pharmacokinetic-related endpoints showed that VGSC interaction was most prominent in RT-3 and RT-1, indicating their potential relevance in neurological targeting. BBB permeability analysis further supported this observation, with RT-5 and RT-3 demonstrating higher permeability, suggesting their suitability for central nervous system drug delivery, while RT-2 and RT-8 showed comparatively lower penetration. For this table RT-5 emerged as the safest compound in terms of acute toxicity, although its higher neurotoxicity and mutagenicity may limit its therapeutic applicability. RT-3 exhibited a balanced profile with strong VGSC interaction and favorable BBB permeability, making it a promising candidate for CNS-related applications. RT-9 demonstrated a comparatively safer hepatic profile and consistent prediction accuracy, indicating its potential as a well-balanced lead compound. In contrast, RT-2 and RT-6 showed relatively unfavorable toxicity characteristics, highlighting the need for structural optimization.

Comparative Physicochemical and Drug-Likeness Analysis

The physicochemical properties of the designed molecules (RT-1 to RT-9) were systematically analysed given in Table 4 to evaluate their drug-likeness and oral bioavailability potential in accordance with established guidelines such as Lipinski's Rule of Five. The molecular formulas indicate structural diversity among the compounds, with variations in heteroatom composition and functional groups that influence their pharmacokinetic behavior. All compounds exhibited an acceptable number of hydrogen bond donors (2-4) and hydrogen bond acceptors (4-8), remaining within the permissible limits for good membrane permeability. Notably, RT-3 showed the highest number of hydrogen bond acceptors (8), which may enhance aqueous solubility but could potentially reduce permeability. In contrast, compounds such as RT-2, RT-5, RT-7, and RT-9 demonstrated a lower number of acceptors (4), suggesting a more balanced polarity profile. Molar Refractivity (MR), an indicator of molecular volume and polarizability, ranged from 138.75 to 164.31, with RT-3 exhibiting the highest value, reflecting its relatively larger and

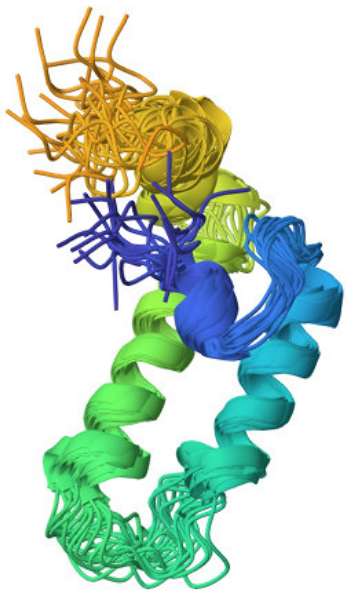

Figure 1: Crystal structure of J-Domain (Residues 2-76) in the N-Terminal Fragment of the Molecular Chaperone.

Table 1: Hydantoin, and its substituted derivative from RT-RT9.

Comp. Code	Structure	Comp. Code	Structure
RT-1	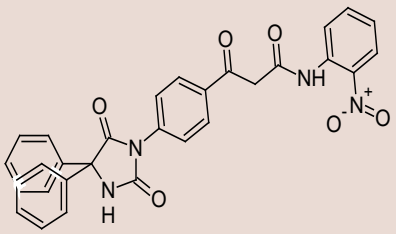	RT-6	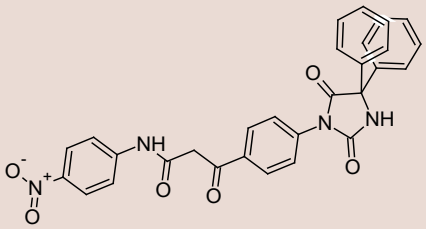
RT-2	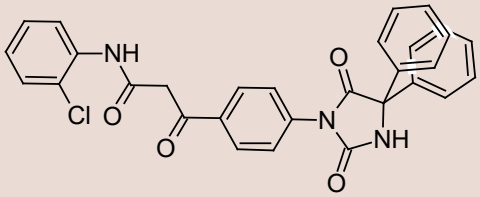	RT-7	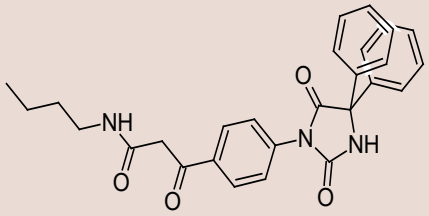
RT-3	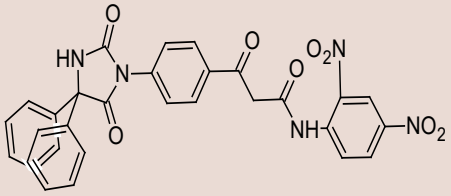	RT-8	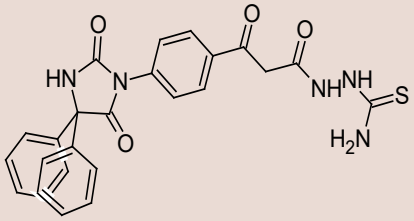
RT-4	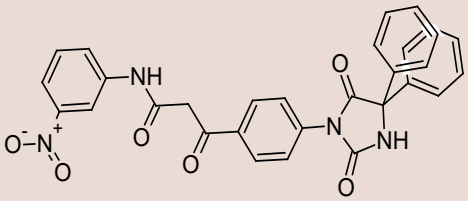	RT-09	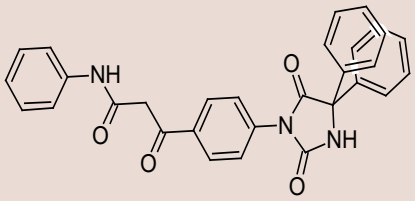
RT-5	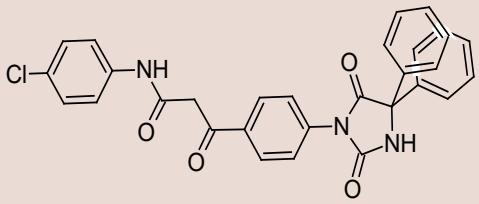		

more polarizable structure. The Topological Polar Surface Area (TPSA), a key determinant of absorption and permeability, varied significantly among the compounds. RT-2, RT-5, RT-7, and RT-9 displayed optimal TPSA values (~95.58 Å²), indicative of favorable intestinal absorption. In contrast, RT-3 (187.22 Å²) and RT-8 (165.72 Å²) exceeded the recommended threshold, suggesting possible limitations in membrane permeability and oral bioavailability. Lipophilicity, as indicated by iLOGP and XLOGP3 values, remained within an acceptable range for most compounds. RT-2 and RT-5 exhibited relatively higher XLOGP3 values (5.74), approaching the upper limit, which may enhance membrane permeability but could also increase the risk of poor solubility. Conversely, RT-8 demonstrated the lowest lipophilicity (iLOGP=2.07; XLOGP3=2.54), indicating better aqueous solubility but potentially reduced permeability. Compounds RT-1, RT-4, RT-6, and RT-9 maintained a balanced lipophilic profile, suggesting optimal absorption characteristics. For this Table analysis, RT-7 and RT-9 demonstrated the most favorable balance of physicochemical parameters, including optimal TPSA, moderate lipophilicity, and acceptable hydrogen bonding capacity, indicating strong drug-likeness potential. In contrast, RT-3 and RT-8 may require structural optimization due to their elevated TPSA values, which could limit bioavailability. These findings highlight the importance of integrating physicochemical profiling in early-stage drug design to identify compounds with optimal pharmacokinetic properties.

Table 2: The six parameters shown are shown as LIPO: Lipophilicity; SIZE: Molecular weight; POLAR: Polarity (TPSA); INSOLU: Insolubility; INSATU: Unsaturation; FLEX: Flexibilit.

Comp Code	Structure	Comp. Code	Structure
RT-1	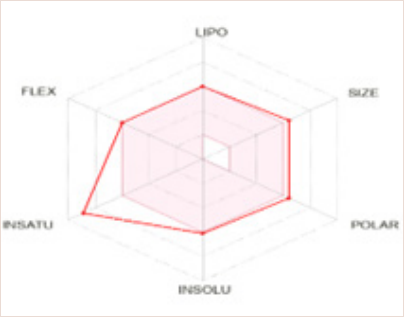	RT-6	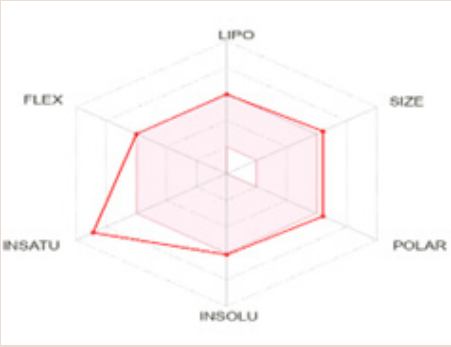
RT-2		RT-7	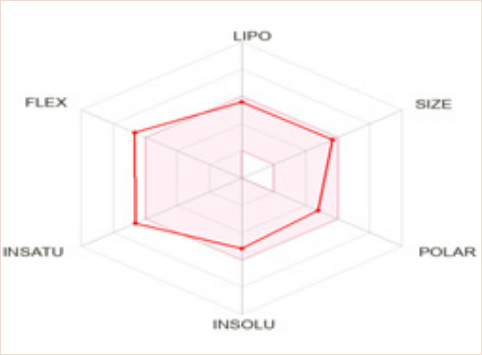
RT-3		RT-8	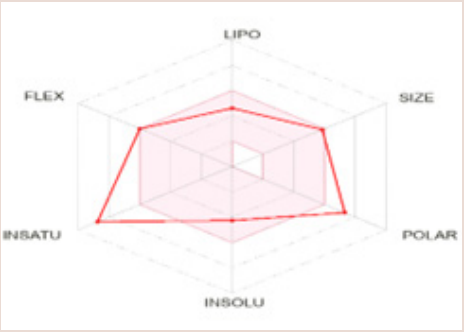
RT-4		RT-09	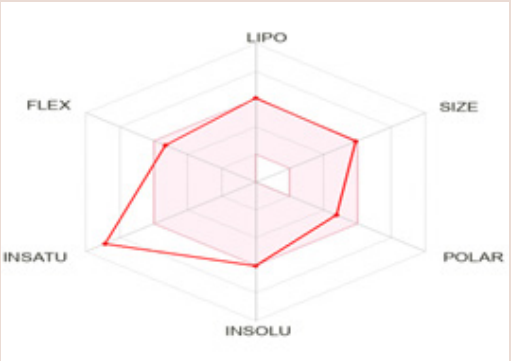

Comp Code	Structure	Comp. Code	Structure
RT-5	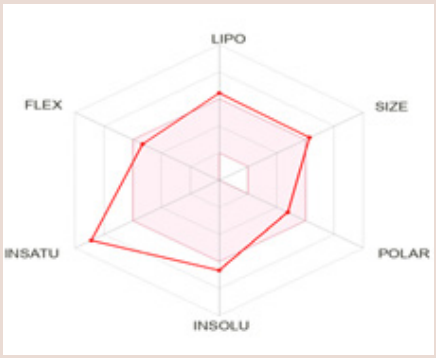		

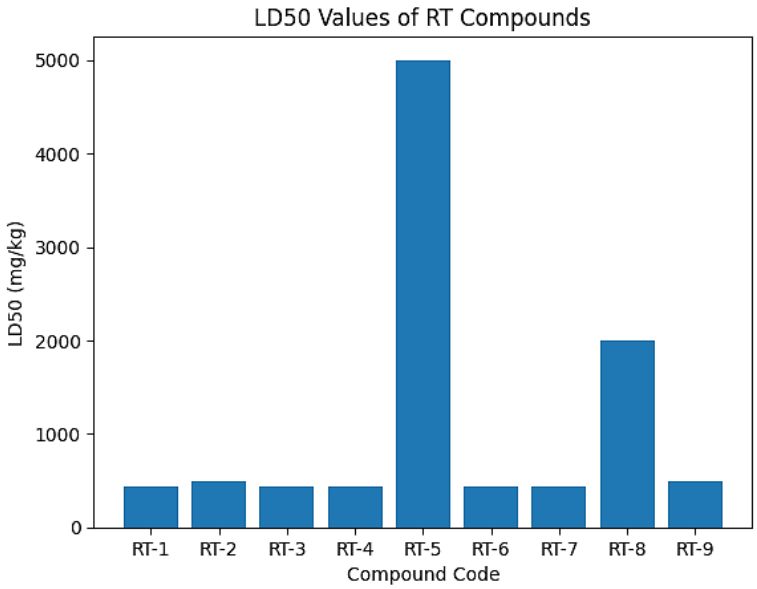

Figure 2: Comparative graph of LD_{50} Value of RT compounds.

Comparative ADMET and Pharmacokinetic Profile Analysis

The pharmacokinetic properties of the designed compounds (RT-1 to RT-9) were evaluated to assess their absorption, distribution, and metabolic interaction profiles given in Table 5 using *in silico* prediction tools such as Swiss-ADME. The analysis revealed notable variations in Gastrointestinal (GI) absorption, P-glycoprotein (P-gp) substrate behavior, and cytochrome P450 (CYP) enzyme inhibition patterns, which are critical determinants of oral bioavailability and metabolic stability. GI absorption analysis indicated that RT-2, RT-5, RT-7, and RT-9 exhibited high absorption, suggesting favorable oral bioavailability, whereas the remaining compounds (RT-1, RT-3, RT-4, RT-6, and RT-8) showed low absorption, potentially limiting their systemic availability. None of the compounds were predicted to be Blood-Brain Barrier (BBB) permeant, indicating limited central nervous system penetration, which may reduce the risk of CNS-related side effects but also limits their applicability for neurological targets. P-gp substrate prediction demonstrated that most compounds are non-substrates, except RT-7, which may be susceptible to efflux mechanisms, potentially reducing intracellular drug accumulation. In terms of metabolic interactions, all compounds were predicted to be non-inhibitors of CYP1A2, suggesting minimal interference with this enzyme. However, a consistent inhibitory effect on CYP2C19 and CYP2C9 was observed across most compounds, indicating a potential for drug-drug interactions. Notably, RT-3 and RT-8 did not inhibit CYP2C19, suggesting a comparatively safer metabolic profile in this aspect. Furthermore, CYP2D6 inhibition was observed only in RT-7, while CYP3A4 inhibition was predicted for RT-3 and RT-7, highlighting possible metabolic liabilities for these compounds. The broader CYP inhibition profile of RT-7, including CYP2C19, CYP2C9, CYP2D6, and CYP3A4, suggests a higher likelihood of pharmacokinetic interactions, making it less favorable compared to other candidates. Overall, RT-2, RT-5, and RT-9 demonstrated the most favorable pharmacokinetic profiles, characterized by high GI absorption and limited CYP enzyme interference. In contrast, RT-7 exhibited multiple metabolic liabilities despite

good absorption, while RT-3 showed selective CYP inhibition and low absorption, indicating the need for further optimization. These findings emphasize the importance of integrating ADMET profiling in early drug development to identify compounds with optimal pharmacokinetic and safety characteristics.

Comparative Drug-Likeness and Bioavailability Analysis

The drug-likeness and bioavailability profiles of the synthesized compounds (RT-1 to RT-9) were evaluated using multiple rule-based filters, including Lipinski's Rule of Five, Ghose, Veber, Egan, and Muegge criteria, along with skin permeability (log Kp) and bioavailability score predictions given in Table 6. These parameters are essential for assessing the suitability of compounds for oral drug development. The predicted skin permeability values (log Kp) ranged from -5.42 to -7.47 cm/s, indicating generally low transdermal permeability across all compounds. Among them, RT-2 and RT-5 (-5.42 cm/s) exhibited relatively higher permeability, while RT-8 (-7.47 cm/s) showed the lowest, suggesting limited dermal absorption potential. Evaluation of Lipinski's rule violations revealed that most compounds exhibited one violation, whereas RT-3 showed two violations, indicating a comparatively less favorable drug-likeness profile. Notably, RT-7, RT-8, and RT-9 demonstrated zero Lipinski violations, suggesting strong compliance with oral drug-likeness criteria. Ghose filter analysis indicated one to two violations across all compounds, with RT-7 showing the least deviation (one violation), further supporting its favorable physicochemical profile. Veber and Egan rule assessments, which are closely associated with oral bioavailability, showed that RT-2, RT-5, RT-7, and RT-9 had no violations, indicating optimal molecular flexibility and polarity. In contrast, RT-1, RT-3, RT-4, RT-6, and RT-8 exhibited one violation each, suggesting moderate limitations in oral absorption. Muegge filter evaluation highlighted that most compounds had either zero or one violation, except RT-3, which showed one violation across multiple filters, indicating the need for structural optimization. The bioavailability score further supported these findings, with most compounds (RT-1, RT-2, RT-4, RT-5, RT-6, RT-7, RT-8, and RT-9) demonstrating a favorable score of 0.55, indicative of good oral bioavailability potential. In contrast,

Table 3: Comparative Toxicity and ADMET Analysis including LD_{50} (mg/kg); Toxicity Class; Prediction Accuracy (%); Hepatotoxicity; Cardiotoxicity; Neurotoxicity; Mutagenicity VGSC; BBB-barrier.

Comp. code	LD_{50} (mg/kg)	Toxicity class	Prediction Accuracy (%)	Hepatotoxicity	Cardiotoxicity	Neurotoxicity	Mutagenicity	VGSC	BBB-barrier
RT-1	440	4	67.38	0.65	0.86	0.60	0.80	0.79	0.72
RT-2	500	4	67.38	0.59	0.89	0.84	0.82	0.58	0.58
RT-3	440	4	54.26	0.64	0.87	0.59	0.79	0.80	0.77
RT-4	440	4	67.38	0.64	0.88	0.59	0.80	0.75	0.74
RT-5	5000	5	67.38	0.59	0.89	0.83	0.82	0.56	0.79
RT-6	440	3	67.38	0.63	0.85	0.75	0.66	0.65	0.75
RT-7	440	4	68.07	0.62	0.85	0.78	0.76	0.68	0.61
RT-8	2000	4	67.38	0.63	0.81	0.62	0.68	0.63	0.58
RT-9	500	4	68.07	0.50	0.89	0.80	0.79	0.61	0.75

Table 4: Comparative Analysis of Physicochemical and Drug-Likeness Properties of Phenothiazine Structure interactions with #Rotatable bonds; #H-bond acceptors; #H-bond donors; MR; TPSA; iLOGP; XLOGP3.

Comp. code	Formula	#H-bond acceptors	#H-bond donors	MR	TPSA	I LOGP	X LOGP3
RT-1	$C_{30}H_{22}N_4O_6$	6	2	155.49	141.4	3.24	4.94
RT-2	$C_{30}H_{22}C_1N_3O_4$	4	2	151.68	95.58	3.63	5.74
RT-3	$C_{30}H_{21}N_5O_8$	8	2	164.31	187.22	2.91	4.77
RT-4	$C_{30}H_{22}N_4O_6$	6	2	155.49	141.4	2.61	4.94
RT-5	$C_{30}H_{22}C_1N_3O_4$	4	2	151.68	95.58	3.29	5.74
RT-6	$C_{30}H_{22}N_4O_6$	6	2	155.49	141.4	2.99	4.94
RT-7	$C_{28}H_{27}N_3O_4$	4	2	139.87	95.58	3.12	4.26
RT-8	$C_{25}H_{21}N_5O_4S$	4	4	138.75	165.72	2.07	2.54
RT-9	$C_{30}H_{23}N_3O_4$	4	2	146.67	95.58	3.47	5.11

Table 5: Comparative Analysis of Pharmacokinetic and ADME Properties.

Comp. code	GI absorption	BBB permeant	Pgp substrate	CYP1A2 inhibitor	CYP2C19 inhibitor	CYP2C9 inhibitor	CYP2D6 inhibitor	CYP3A4 inhibitor
RT-1	Low	No	No	No	Yes	Yes	No	No
RT-2	High	No	No	No	Yes	Yes	No	No
RT-3	Low	No	No	No	No	Yes	No	Yes
RT-4	Low	No	No	No	Yes	Yes	No	No
RT-5	High	No	No	No	Yes	Yes	No	No
RT-6	Low	No	No	No	Yes	Yes	No	No
RT-7	High	No	Yes	No	Yes	Yes	Yes	Yes
RT-8	Low	No	No	No	No	Yes	No	No
RT-9	High	No	No	No	Yes	Yes	No	No

Table 6: Comparative Analysis of Pharmacokinetic and ADME Properties.

Comp. code	log Kp (cm/s)	Lipinski #violations	Ghose #violations	Veber #violations	Egan #violations	Muegge #violations	Bioavailability Score
RT-1	-6.05	1	2	1	1	0	0.55
RT-2	-5.42	1	2	0	0	1	0.55
RT-3	-6.45	2	2	1	1	1	0.17
RT-4	-6.05	1	2	1	1	0	0.55
RT-5	-5.42	1	2	0	0	1	0.55
RT-6	-6.05	1	2	1	1	0	0.55
RT-7	-6.14	0	1	0	0	0	0.55
RT-8	-7.47	0	2	1	1	1	0.55
RT-9	-5.66	0	2	0	0	1	0.55

RT-3 exhibited a significantly lower score (0.17), reflecting poor predicted bioavailability and reduced drug-likeness. Overall, RT-7 and RT-9 emerged as the most promising candidates, exhibiting minimal rule violations and favorable bioavailability scores. RT-2 and RT-5 also demonstrated acceptable profiles with good permeability and no Veber/Egan violations. Conversely, RT-3 showed multiple violations across different filters and a low bioavailability score, indicating that it may require further structural refinement. These results emphasize the importance of integrating multiple drug-likeness criteria to identify compounds with optimal pharmacokinetic properties for further development.

3D Amino Acid Interaction Analysis

The 3D visualization of ligand-protein complexes given in Table 7 reveals that the docked compounds are well accommodated within the active binding pocket, forming multiple stabilizing interactions with surrounding amino acid residues. In this structure, the ligand is deeply embedded within the binding cavity and forms several hydrogen bonds (green dashed lines) with nearby polar residues. These interactions appear to involve key amino acids such as ASN, GLU, and SER, which are known to contribute to binding specificity through strong donor-acceptor interactions. Additionally, hydrophobic interactions (pink/purple dashed lines) are observed between the aromatic rings of the ligand and non-polar residues, enhancing van der Waals stabilization. The presence of π-π stacking and π-alkyl interactions with aromatic residues further strengthens ligand binding. In this structure, the ligand adopts a slightly different conformation but maintains strong binding through a combination of hydrogen bonding, electrostatic, and hydrophobic interactions. The yellow/orange dashed lines indicate electrostatic interactions, likely involving charged residues such as ARG and ASP, which play a crucial role in ligand orientation and binding affinity. The aromatic moieties of the ligand are positioned favorably within hydrophobic pockets, forming π-π and π-cation interactions, particularly with residues like TYR, TRP, or PHE. All 3D structures demonstrate that Hydrogen bonds ensure specificity and proper anchoring of the ligand; Hydrophobic interactions stabilize the ligand within the binding pocket; Electrostatic interactions contribute to binding strength and orientation; Aromatic interactions (π-π stacking) enhance overall complex stability. These combined interactions indicate that the ligand exhibits a stable and energetically favorable binding mode, supporting the docking results and reinforcing its potential as a promising candidate for further studies.

Table 7: Multiple interactions involving different amino acids; Hydrogen Bond; Electrostatic and Hydrophobic interactions by RT1 -RT9 molecules.

Comp Code	3D	Comp Code	3D
RT-1	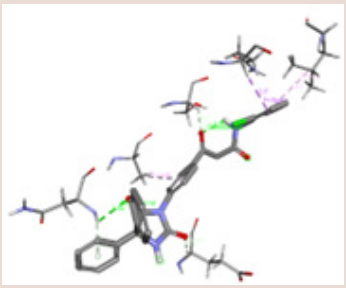	RT-6	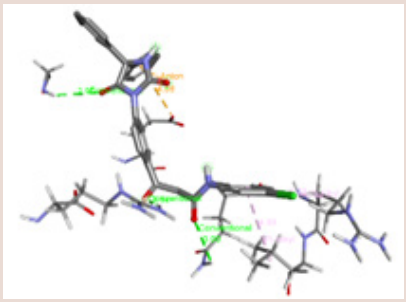
RT-2	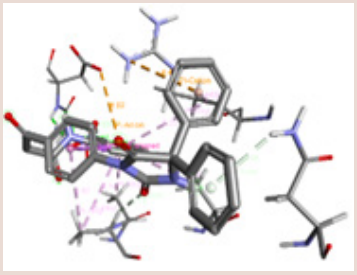	RT-7	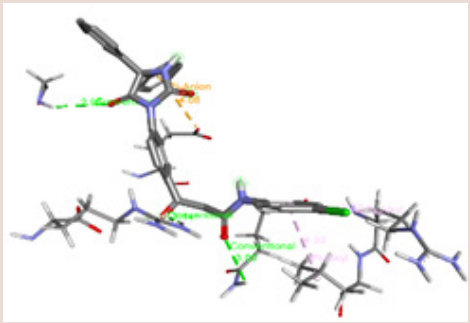
RT-3	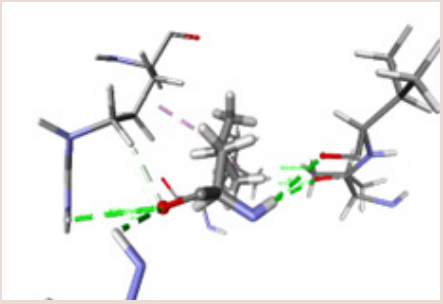	RT-8	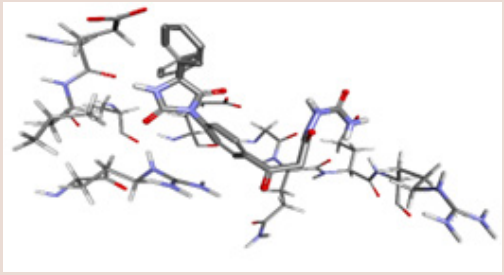
RT-4	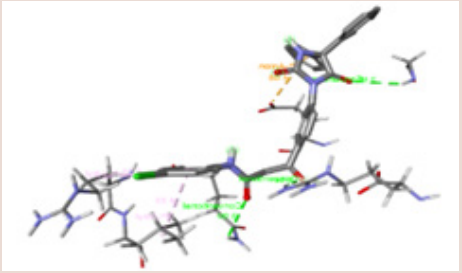	RT-9	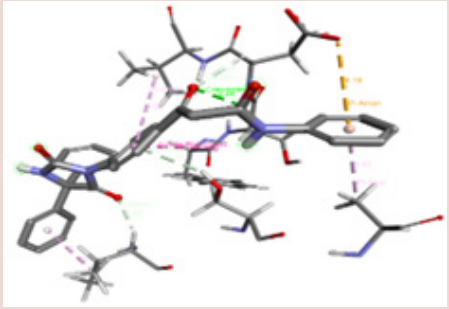
RT-5	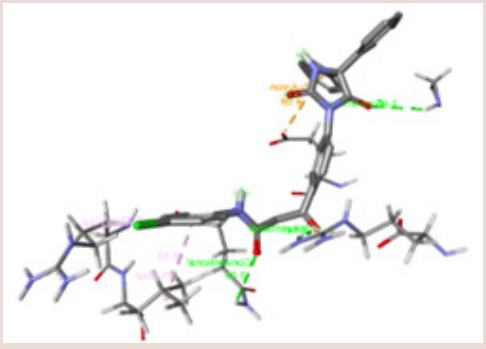		

Molecular docking analysis and amino acid Evaluations

The molecular docking analysis of the designed compounds (RT-1 to RT-9) demonstrated significant binding affinity toward the target protein given in Table 8 as reflected by favorable docking scores ranging from -6.9 to -7.9 kcal/mol. Among the evaluated ligands, RT-3, RT-4, and RT-5 exhibited the highest binding affinity (-7.9 kcal/mol), indicating strong and stable interactions within the active site of the protein. A detailed interaction analysis revealed that hydrogen bonding plays a critical role in stabilizing ligand-protein complexes. Compounds RT-1, RT-2, RT-3, RT-5, RT-6, and RT-8 formed multiple hydrogen bonds with key amino acid residues such as ASN197, GLU193, SER203, GLN207, ASP29, and ARG587. Notably, RT-8 exhibited the highest number of hydrogen bonds, suggesting enhanced binding stability despite having a comparatively moderate docking score (-7.1 kcal/mol). This indicates that binding affinity is not solely dependent on the number of hydrogen bonds but also on the overall interaction profile. Hydrophobic interactions were also observed to significantly contribute to ligand stabilization within the binding pocket. Residues such as LEU130, VAL126, PHE123, TYR173, and TRP169 were frequently involved in hydrophobic and π-alkyl interactions, particularly in RT-3, RT-4, and RT-7. These interactions enhance ligand accommodation in the hydrophobic regions of the protein, thereby improving binding affinity. Electrostatic interactions further supported complex stability in several compounds. RT-2, RT-4, RT-5, and RT-9 exhibited interactions involving charged residues such as ASP29, GLU124, and ARG165/ARG587. These interactions are crucial for proper ligand orientation and contribute to stronger binding through charge complementarity. Among all compounds, RT-3 demonstrated a balanced interaction profile, involving multiple hydrogen bonds along with hydrophobic interactions,

Table 8: Multiple interactions involving different amino acids; Hydrogen Bond; Electrostatic and Hydrophobic interactions by RT1 -RT9 molecules.

Sl. No.	Name	Distance	Category	Hydrogen Donor	Hydrogen Acceptor	Dock score
RT-1	A:ASN197	2.89226	Hydrogen Bond	H-Donor	H-Acceptor	-7.6
	A:GLU193	2.28532	Hydrogen Bond	H-Donor	H-Acceptor	
	A:SER203	2.5658	Hydrogen Bond	H-Donor	H-Acceptor	
	A:ASN197	2.61006	Hydrogen Bond	H-Donor	H-Acceptor	
	A:GLN207	2.72396	Hydrogen Bond	H-Donor	Pi-Orbitals	
	A:ALA199	2.80918	Hydrophobic	C-H	Pi-Orbitals	
	A:LEU210	4.41182	Hydrophobic	Pi-Orbitals	Alkyl	
			Hydrophobic	Pi-Orbitals	Alkyl	
RT-2	A:ASP29	2.68066	Hydrogen Bond	H-Donor	H-Acceptor	-7.8
	A:SER28	2.85019	Hydrogen Bond	H-Donor	H-Acceptor	
	A:ALA168	2.74451	Hydrogen Bond	H-Donor	H-Acceptor	
	A:ARG6	4.46552	Electrostatic	Positive	Pi-Orbitals	
	A:ASP29	4.81924	Electrostatic	Negative	Pi-Orbitals	
	A:ASN175	3.23618	Hydrogen Bond	H-Donor	Pi-Orbitals	
		3.70316	Hydrophobic	C-H	Pi-Orbitals	
RT-3	A:LEU130	2.31777	Hydrogen Bond	H-Donor	H-Acceptor	-7.9
	A:VAL126	2.8304	Hydrogen Bond	H-Donor	H-Acceptor	
	A:LEU130	2.35214	Hydrogen Bond	H-Donor	H-Acceptor	
	A:VAL127	3.08157	Hydrogen Bond	H-Donor	H-Acceptor	
	A:ARG132	2.24188	Hydrogen Bond	H-Donor	H-Acceptor	
	A:LEU130	5.07424	Hydrophobic	Alkyl	Alkyl	
	A:ARG139	3.89371	Hydrophobic	Alkyl	Alkyl	
	A:LEU130					
	A:ARG139					
	A:LEU130					
	A:LEU130					
	B:LEU578					
	A:ARG139					
	A:LEU130					

Sl. No.	Name	Distance	Category	Hydrogen Donor	Hydrogen Acceptor	Dock score
RT-4	A:TRP169	2.19416	Hydrogen Bond	H-Donor	H-Acceptor	-7.9
	A:TYR173	2.31798	Hydrogen Bond	H-Donor	H-Acceptor	
	A:GLU124	3.46951	Electrostatic	Negative	Pi-Orbitals	
	A:TRP169	4.86399	Hydrophobic	Pi-Orbitals	Pi-Orbitals	
	A:HIS177	4.40074	Hydrophobic	Pi-Orbitals	Pi-Orbitals	
	A:TRP169	4.96399	Hydrophobic	Pi-Orbitals	Pi-Orbitals	
	A:ARG165	4.89716	Hydrophobic	Pi-Orbitals	Alkyl	
RT-5	A:GLY196	2.9474	Hydrogen Bond	H-Donor	H-Acceptor	-7.9
	A:GLN207	2.99817	Hydrogen Bond	H-Donor	H-Acceptor	
	B:ARG587	2.14316	Hydrogen Bond	H-Donor	H-Acceptor	
	B:ARG587	1.95676	Hydrogen Bond	H-Donor	H-Acceptor	
	A:GLU202	4.07651	Electrostatic	Negative	Pi-Orbitals	
	A:ARG209	5.33422	Hydrophobic	Pi-Orbitals	Alkyl	
	A:LEU210	4.33428	Hydrophobic	Pi-Orbitals	Alkyl	
RT-6	A:GLN207:	2.87661	Hydrogen Bond	H-Donor	H-Acceptor	-7.5
	B:ARG587	2.58041	Hydrogen Bond	H-Donor	H-Acceptor	
	A:SER203	2.7313	Hydrogen Bond	H-Donor	H-Acceptor	
	A:SER203	2.39581	Hydrogen Bond	H-Donor	H-Acceptor	
RT-7	A:GLU124	3.64732	Hydrogen Bond	H-Donor	H-Acceptor	-6.9
	A:TYR120	3.91096	Hydrophobic	Pi-Orbitals	Pi-Orbitals	
	A:TRP169	4.96675	Hydrophobic	Pi-Orbitals	Pi-Orbitals	
	A:GLY117	4.35986	Hydrophobic	Amide	Pi-Orbitals	
	A-THR118	5.34279	Hydrophobic	Pi-Orbitals	Alkyl	
	A:PHE123	5.05277	Hydrophobic	Pi-Orbitals	Alkyl	
	A:TYR173	5.07938	Hydrophobic	Pi-Orbitals	Alkyl	
	A:TYR173					
RT-8	B:ARG587:	2.91156	Hydrogen Bond	H-Donor	H-Acceptor	-7.1
	B:ARG587:	2.62366	Hydrogen Bond	H-Donor	H-Acceptor	
	A:GLU193:O	2.38717	Hydrogen Bond	H-Donor	H-Acceptor	
	A:GLY206:O	2.29141	Hydrogen Bond	H-Donor	H-Acceptor	
	A:GLN207:O	2.30996	Hydrogen Bond	H-Donor	H-Acceptor	
	A:GLY206:O	2.15744	Hydrogen Bond	H-Donor	H-Acceptor	
		2.50457	Hydrogen Bond	H-Donor	H-Acceptor	
RT-9	A:ASP29	2.45631	Hydrogen Bond	H-Donor	H-Acceptor	-7.7
	A:ASP29	2.47079	Hydrogen Bond	H-Donor	H-Acceptor	
	A:VAL161	2.23661	Hydrogen Bond	H-Donor	H-Acceptor	
	A:ASP29	4.1931	Electrostatic	Negative	Pi-Orbitals	
	A:SER164	3.07466	Hydrogen Bond	H-Donor	Pi-Orbitals	
	A:PHE27	4.82912	Hydrophobic	Amide	Pi-Orbitals	
	A-SER28	5.35024	Hydrophobic	Pi-Orbitals	Alkyl	
	A:VAL30					

particularly with residues LEU130 and ARG139. Similarly, RT-4 and RT-5 showed strong binding due to a combination of hydrogen bonding, electrostatic, and hydrophobic interactions, indicating their potential as promising lead compounds. On the other hand, RT-7 showed the lowest docking score (-6.9 kcal/mol), which may be attributed to the predominance of hydrophobic interactions and fewer stabilizing hydrogen bonds. This suggests comparatively weaker binding affinity and reduced

stability within the active site. Overall, the docking results suggest that an optimal combination of hydrogen bonding, hydrophobic interactions, and electrostatic forces is essential for strong ligand binding. Compounds RT-3, RT-4, and RT-5, in particular, demonstrated superior interaction profiles and binding energies, highlighting their potential for further optimization and *in vitro* validation.

DISCUSSION

The present study provides a comprehensive *in silico* evaluation of hydantoin-based derivatives (RT-1 to RT-9) for their potential anticonvulsant activity using molecular docking and ADMET profiling. The integration of these computational approaches offers valuable insights into ligand-protein interactions, pharmacokinetic behavior, and toxicity, which are essential parameters in early-stage drug discovery. Molecular docking results demonstrated that all designed compounds exhibited moderate to strong binding affinity toward the target protein (PDB ID: 1XBL), with docking scores ranging from -6.9 to -7.9 kcal/mol. Among them, RT-3, RT-4, and RT-5 showed the most favorable binding energies, suggesting stable ligand-protein complex formation. The superior binding affinity of these compounds can be attributed to their ability to establish multiple stabilizing interactions within the active site. Hydrogen bonding emerged as a key determinant of binding specificity, particularly involving amino acid residues such as ASN197, GLU193, SER203, and GLN207. These interactions facilitate proper ligand orientation and anchoring within the binding pocket. In addition to hydrogen bonding, hydrophobic interactions significantly contributed to ligand stability. Residues such as LEU130, VAL126, TRP169, and TYR173 were frequently involved in π-alkyl and van der Waals interactions, enhancing the overall binding affinity. Electrostatic interactions with charged residues, including ARG and ASP, further strengthened ligand binding by providing additional stabilization through charge complementarity. Notably, RT-3 exhibited a well-balanced interaction profile, combining hydrogen bonding and hydrophobic interactions, which explains its high docking score and stable binding conformation. Interestingly, RT-8 formed the highest number of hydrogen bonds but did not achieve the best docking score, highlighting that binding affinity is not solely dependent on hydrogen bonding. Instead, an optimal combination of hydrogen bonding, hydrophobic interactions, and electrostatic forces is required for strong and stable ligand binding. Conversely, RT-7 exhibited the lowest binding affinity (-6.9 kcal/mol), likely due to fewer hydrogen bonds and a predominance of weaker hydrophobic interactions, resulting in reduced stability within the active site. The ADMET analysis provided further insights into the pharmacokinetic and toxicity profiles of the compounds. RT-5 demonstrated the highest LD_{50} value (5000 mg/kg), indicating low acute toxicity and suggesting a favorable safety profile. However, its relatively higher neurotoxicity and mutagenicity values may pose limitations for therapeutic application. In contrast, RT-9 exhibited the lowest hepatotoxicity and a balanced toxicity profile, making it a safer candidate among the evaluated compounds. Most compounds showed moderate toxicity, which is typical for early-stage drug candidates and may be improved through structural optimization. Pharmacokinetic evaluation revealed that RT-2, RT-5, RT-7, and RT-9 possess high gastrointestinal absorption, indicating good oral bioavailability. However, none of the compounds were predicted to permeate the Blood-Brain Barrier (BBB), which may limit their effectiveness in treating central nervous system disorders such as epilepsy. This limitation suggests that further structural modifications may be required to enhance BBB permeability while maintaining favorable pharmacokinetic properties. The Cytochrome P450 (CYP) inhibition profile indicated that most compounds inhibit CYP2C19 and CYP2C9, which may lead to potential drug-drug interactions. RT-7, in particular, exhibited inhibition of multiple CYP isoforms, including CYP2D6 and CYP3A4, indicating a higher risk of metabolic complications. In contrast, RT-3 and RT-8 showed relatively fewer CYP interactions, suggesting a comparatively safer metabolic profile. Drug-likeness assessment using Lipinski, Veber, and Egan rules further supported the pharmacokinetic findings. RT-7 and RT-9 demonstrated minimal rule violations and favorable bioavailability scores, indicating strong potential as orally active drug candidates. On the other hand, RT-3 exhibited multiple violations and a lower bioavailability score, suggesting limitations in absorption despite its strong binding affinity. This highlights the importance of balancing physicochemical properties with biological activity during drug design. The results emphasize that molecular docking alone is insufficient for identifying promising drug candidates. Instead, a combined approach integrating docking, ADMET, and drug-likeness analysis is essential for accurate lead optimization. Compounds such as RT-3, RT-5, and RT-9 demonstrated promising characteristics; however, each exhibits specific limitations that require further refinement. These findings provide a strong foundation for future experimental validation and optimization studies aimed at developing effective anticonvulsant agents.

CONCLUSION

The present *in silico* study successfully evaluated the anticonvulsant potential of hydantoin-based derivatives using molecular docking and ADMET analysis. The results demonstrated that compounds RT-3, RT-4, and RT-5 exhibit strong binding affinity toward the target protein 1XBL, supported by multiple stabilizing interactions such as hydrogen bonding, hydrophobic contacts, and electrostatic interactions. Among all compounds, RT-3 emerged as a promising candidate due to its balanced interaction profile and favorable VGSC interaction, despite some limitations in bioavailability. RT-5 showed the lowest toxicity but requires further evaluation due to higher neurotoxicity and mutagenicity. RT-9 demonstrated an optimal balance

between safety, pharmacokinetics, and drug-likeness, making it a strong candidate for further development. The ADMET and drug-likeness analyses revealed that RT-7 and RT-9 possess the most favorable pharmacokinetic properties, while RT-3 requires structural optimization due to poor bioavailability. These findings emphasize that both binding affinity and pharmacokinetic properties must be considered simultaneously in drug design. In conclusion, compounds RT-3, RT-5, and RT-9 can be considered promising lead molecules for anticonvulsant drug development. However, further *in vitro* and *in vivo* studies are necessary to validate their efficacy and safety. The integration of molecular docking and ADMET profiling proves to be a powerful and cost-effective strategy for identifying and optimizing potential therapeutic candidates for Paroxysmal Neurological Disorders.

ACKNOWLEDGEMENT

The authors are thankful to Pravara Rural College of Pharmacy, Pravaranagar.

ABBREVIATIONS

ADME: Absorption, distribution, metabolism, and excretion; **BBB:** Blood-brain barrier; **CNS:** Central nervous system; **CYP:** Cytochrome P450; **CYP1A2:** Cytochrome P450 1A2; **CYP2C19:** Cytochrome P450 2C19; **CYP2C9:** Cytochrome P450 2C9; **CYP2D6:** Cytochrome P450 2D6; **CYP3A4:** Cytochrome P450 3A4; **GI:** Gastrointestinal; **HBA:** Hydrogen bond acceptor; **HBD:** Hydrogen bond donor; **Log Kp:** Logarithm of skin permeation coefficient; **LogP:** Logarithm of octanol-water partition coefficient; **MW:** Molecular weight; **PSA:** Polar surface area; **SA Score:** Synthetic accessibility score.

CONFLICT OF INTEREST

The authors declare that there is no conflict of interest.

REFERENCES

Benet, L. Z., Broccatelli, F., and Oprea, T. I. (2016). BDDCS applied to prediction of drug disposition. Pharmaceutical Research, 33, 2545-2554. https://doi.org/10.1007/s11095-016-2000-4

Bleakley, K., and Yamanishi, Y. (2009). Supervised prediction of drug-target interactions. Bioinformatics, 25(18), 2397-2403. https://doi.org/10.1093/bioinformatics/btp433

Cheng, T., Li, Q., Zhou, Z., Wang, Y., and Bryant, S. H. (2012). Structure-based virtual screening for drug discovery. Journal of Chemical Information and Modeling, 52(11), 3099-3105. https://doi.org/10.1021/ci300367a

Daina, A., Michielin, O., and Zoete, V. (2017). SwissADME: Evaluation of pharmacokinetics. Scientific Reports, 7, 42717. https://doi.org/10.1038/srep42717

DiMasi, J. A., Grabowski, H. G., and Hansen, R. W. (2016). Innovation in pharmaceutical industry. Journal of Health Economics, 47, 20-33. https://doi.org/10.1016/j.jhealeco.2016.01.012

Ferreira, L. G., dos Santos, R. N., Oliva, G., and Andricopulo, A. D. (2015). Molecular docking and structure-based drug design. Molecules, 20(7), 13384-13421. https://doi.org/10.3390/molecules200713384

Ghose, A. K., Viswanadhan, V. N., and Wendoloski, J. J. (1999). Drug-like properties database. Journal of Combinatorial Chemistry, 1(1), 55-68. https://doi.org/10.1021/cc9800071

Gleeson, M. P. (2008). Generation of a set of simple rules for drug safety. Journal of Medicinal Chemistry, 51(4), 817-834. https://doi.org/10.1021/jm701122q

Hitchcock, S. A., and Pennington, L. D. (2006). Structure-brain exposure relationships. Journal of Medicinal Chemistry, 49(26), 7559-7583. https://doi.org/10.1021/jm0606423

Hughes, J. D., Blagg, J., Price, D. A., Bailey, S., Decrescenzo, G., Devraj, R. V., Ellsworth, E., Fobian, Y., Gibbs, M. E., Gilles, R. W., Greene, N., Huang, E., Krieger-Burke, T., Loesel, J., Wager, T., Whiteley, L., and Zhang, Y. (2008). Physicochemical drug properties. Bioorganic and Medicinal Chemistry Letters, 18(17), 4872-4875. https://doi.org/10.1016/j.bmcl.2008.07.071

Kapetanovic, I. M. (2008). Computer-aided drug discovery and development. Chemical Biology and Drug Design, 71(2), 165-176. https://doi.org/10.1111/j.1747-0285.2007.00630.x

Kirchmair, J., Göller, A. H., Lang, D., Kunze, J., Testa, B., Wilson, I. D., Glen, R. C., and Schneider, G. (2012). Predicting drug metabolism. Nature Reviews Drug Discovery, 11, 387-404. https://doi.org/10.1038/nrd3701

Kitchen, D. B., Decornez, H., Furr, J. R., and Bajorath, J. (2004). Docking and scoring in virtual screening. Nature Reviews Drug Discovery, 3(11), 935-949. https://doi.org/10.1038/nrd1549

Kwan, P., and Brodie, M. J. (2000). Early identification of refractory epilepsy. New England Journal of Medicine, 342, 314-319. https://doi.org/10.1056/NEJM200002033420503

Lionta, E., Spyrou, G., Vassilatis, D. K., and Cournia, Z. (2014). Structure-based drug design. Current Topics in Medicinal Chemistry, 14(16), 1923-1938. https://doi.org/10.2174/1568026614666140929124445

Lipinski, C. A. (2004). Lead- and drug-like compounds. Drug Discovery Today, 9(8), 337-341. https://doi.org/10.1016/S1359-6446(04)03023-6

Löscher, W. (2011). Mechanisms of drug resistance in epilepsy. Nature Reviews Neuroscience, 12(7), 412-424. https://doi.org/10.1038/nrn3049

Morris, G. M., Huey, R., Lindstrom, W., Sanner, M. F., Belew, R. K., Goodsell, D. S., and Olson, A. J. (2009). AutoDock4 and AutoDockTools4. Journal of Computational Chemistry, 30(16), 2785-2791. https://doi.org/10.1002/jcc.21256

Pardridge, W. M. (2012). Drug transport across the blood-brain barrier. NeuroRx, 2(1), 3-14. https://doi.org/10.1602/neurorx.2.1.3

Pires, D. E. V., Blundell, T. L., and Ascher, D. B. (2015). pkCSM: Predicting pharmacokinetic properties. Journal of Medicinal Chemistry, 58(9), 4066-4072. https://doi.org/10.1021/acs.jmedchem.5b00104

Rang, H. P., Ritter, J. M., Flower, R. J., and Henderson, G. (2015). Rang and Dale's pharmacology (8th ed.). Elsevier. https://doi.org/10.1016/C2009-0-00093-6

Rogawski, M. A. (2006). Ion channels as targets for antiepileptic drugs. Epilepsy Research, 69(3), 273-294. https://doi.org/10.1016/j.eplepsyres.2006.02.005

Shoichet, B. K. (2004). Virtual screening of chemical libraries. Nature, 432, 862-865. https://doi.org/10.1038/nature03197

Trott, O., and Olson, A. J. (2010). AutoDock Vina. Journal of Computational Chemistry, 31(2), 455-461. https://doi.org/10.1002/jcc.21334

Veber, D. F., Johnson, S. R., Cheng, H. Y., Smith, B. R., Ward, K. W., and Kopple, K. D. (2002). Molecular properties affecting bioavailability. Journal of Medicinal Chemistry, 45(12), 2615-2623. https://doi.org/10.1021/jm020017n

Cite this article: Thorat RR, Bhor RJ, Bhosale MS, Thorat YR, Bhoite NA, Algude AV, *et al*. *In silico* Evaluation of Paroxysmal Neurological Disorders Using Molecular Docking Analysis of Hydantoin-Based Compounds Targeting Protein 1XBL for Anticonvulsant Activity. Asian J Biol Life Sci. 2026;15(2):332-45.